PHYSICAL REVIEW B **90**, 075404 (2014)

Plasmonic surface lattice resonances on arrays of different lattice symmetry

Alastair D. Humphrey[1] and William L. Barnes[1,2]
[1]*School of Physics and Astronomy, University of Exeter, Exeter, EX4 4QL, United Kingdom*
[2]*Complex Photonic Systems (COPS), MESA+ Institute for Nanotechnology, University of Twente, 7500 AE Enschede, The Netherlands*
(Received 19 May 2014; revised manuscript received 17 July 2014; published 7 August 2014)

Arrays of metallic particles may exhibit optical collective excitations known as surface lattice resonances (SLRs). These SLRs occur near the diffraction edge of the array and can be sharper than the plasmon resonance associated with the isolated single particle response. We have fabricated and modeled arrays of silver nanoparticles of different geometries. We show that square, hexagonal, and honeycomb arrays show similar SLRs; no one geometry shows a clear advantage over the others in terms of resonance linewidth. We investigate the nature of the coupling between the particles by looking at rectangular arrays. Our results combine experiment and modeling based on a simple coupled-dipole model.

DOI: 10.1103/PhysRevB.90.075404 PACS number(s): 42.25.Fx, 71.45.Gm, 73.20.Mf, 78.67.Bf

I. INTRODUCTION

Particle plasmons are collective oscillations typically involving the free conduction electrons of a subwavelength metallic particle. These charge density oscillations can be excited by the application of an oscillating external electric field (light), displacing the electrons from their equilibrium positions. The resulting electron motion leads to resonant absorption and scattering of the incident light and high electric field enhancements on the surface of the particle [1]. The spectral position of these resonances depends on the material from which the particle is made, the size, and the shape of the particles [2,3] and on the surrounding dielectric environment [4].

When metallic nanoparticles are placed in a wavelength-scale array for which the array period matches the wavelength of the particle plasmon resonance, an additional resonance may arise, known as a surface lattice resonance (SLR). Reports predicting SLRs go back nearly 30 years [5–8]. Early experiments to see this effect were met with only limited success [9–11], but sharp extinction features arising from SLRs associated with square arrays were eventually reported in 2008 [12–14].

Since these initial experimental reports, interest in exploring the optical response of arrays of plasmonic particles has increased. Investigations have explored, for example, the effect of disorder on the SLRs [15]. More recent work has involved looking at the effect that the number of particles that comprise an array has on the SLR [16], while Zhou and Odom explored out-of-plane resonances [17]. SLRs associated with metal nanoparticle arrays are also interesting due to the way their modes interact with emissive species such as fluorescent molecules, both with regard to light emission [18], and with regard to strong coupling between lattice resonances and quantum emitters [19,20]. Metal nanoparticle arrays are important in plasmonic metamaterials [21], and SLRs have been explored in the context of topological metamaterials [22].

One aspect of surface lattice resonances that has seen little investigation is the role of lattice symmetry. In this paper we compare the SLRs of square, rectangular, hexagonal, and honeycomb arrays. We use electron-beam lithography (EBL) to fabricate arrays of metallic nanoparticles and characterize them by measuring normal incidence optical transmittance, thereby allowing us to determine the extinction of the arrays. In addition, we use a coupled dipole model to simulate the extinction. Comparison of the results of experiment and simulation allow us to better understand the nature of the SLRs these structures support.

The optical response of a metallic nanoparticle may be usefully considered from the perspective of the particle's polarizability, in particular the extinction cross section is easily derived from the polarizability [23,24]. The typical size of the particles in the work reported here was too large (size/$\lambda \sim 0.1$) to allow the simplest approximation for the polarizability, i.e., the quasistatic polarizability, to be used. The quasistatic approach does not include any retardation effects, it is thus only valid for particlesizes $\ll\lambda$. For the particles considered here retardation needs to be taken into account. A complete solution to the problem makes use of the full Maxwell equations in what is known as Mie theory [25]. The disadvantage of Mie theory is that it does not lend itself easily to constructing a simple model for the response of arrays of particles. A convenient and often adopted alternative is the modified long-wavelength approximation (MLWA). The MLWA approach builds on the quasistatic polarizability by adding two extra terms, one for dynamic depolarization [26] and one for radiation damping [27]. Dynamic depolarization arises from the fact that the electric field produced by the charge distribution on one part of a particle is retarded with respect to that produced on another part. Radiation damping arises because the accelerating charges associated with the dipole moment of the particles produces electromagnetic radiation. The polarizability in the MLWA is given by [28]

$$\alpha_{\mathrm{MLWA}} = \frac{\alpha_{\mathrm{static}}}{1 - \frac{2}{3}ik^3\alpha_{\mathrm{static}} - \frac{k^2}{a}\alpha_{\mathrm{static}}}, \tag{1}$$

where k is the wave vector in the medium, a is the semiaxis of the particle parallel to the incident electric field, and α_{static} is the electrostatic polarizability which is given by [23]

$$\alpha_{\mathrm{static}} = abc\frac{\varepsilon_m - \varepsilon_s}{3\varepsilon_s + 3L(\varepsilon_m - \varepsilon_s)}, \tag{2}$$

where a, b, and c are the semiaxes of the particle, ε_s is the relative permittivity of the surrounding medium, ε_m is the

relative permittivity of the material from which the particle is made, and L is a shape factor.

When identical particles are placed in an array their polarizability is modified; the modification arises because incident radiation scattered by one particle may act to drive another. Particles thus experience driving fields due to the incident light and due to light scattered by all of the other particles in the array. We may write the modified susceptibility α^* as [13,16,29]

$$\alpha^* = \frac{1}{1/\alpha - S}, \tag{3}$$

where S is an array factor that depends on the particle separation and arrangement. The array factor S is given by

$$S = \sum_j \exp(ikr_j)\left[\frac{(1-ikr_j)(3\cos^2\theta_j - 1)}{r_j^3} + \frac{k^2\sin^2\theta_j}{r_j}\right], \tag{4}$$

where r_j is the distance from the central particle to particle j and θ_j is the angle between $\vec{r}_j$ and the dipole moment of particle j. Once the polarizability has been calculated, the absorption C_{abs} and scattering C_{scat} cross sections can be found using [23]

$$C_{\text{abs}} = 4\pi k \text{Im}(\alpha) \tag{5}$$

and

$$C_{\text{scat}} = \tfrac{8}{3}\pi k^4 |\alpha|^2, \tag{6}$$

from which the extinction cross section can be calculated:

$$C_{\text{ext}} = C_{\text{abs}} + C_{\text{scat}}. \tag{7}$$

Figure 1 shows the calculated extinction cross sections of a single isolated particle and of a particle in a 480 nm pitch square array. The particles are silver disks (modeled as spheroids) with a diameter of 120 nm and a height of 30 nm immersed in a homogenous medium of refractive index $n = 1.515$, with the electric field in the plane of the particles.

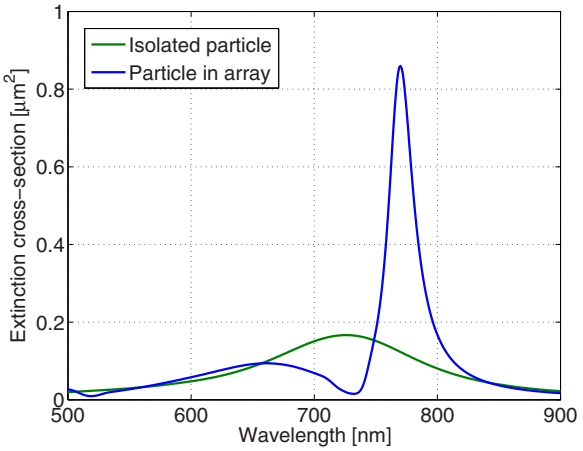

FIG. 1. (Color online) Calculated extinction cross section per particle (μm^2) vs wavelength (nm) of a single isolated particle and a particle in a 480 nm square lattice. The particles are silver disks (spheroids) with a diameter of 120 nm and a height of 30 nm embedded in a homogeneous medium with refractive index $n = 1.515$. The electric field is in the plane of the particles.

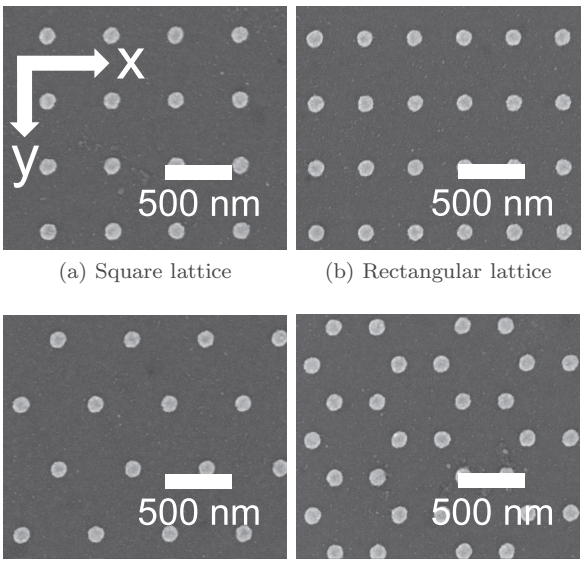

(a) Square lattice (b) Rectangular lattice

(c) Hexagonal lattice (d) Honeycomb lattice

FIG. 2. Scanning electron micrographs (SEMs) of different arrays of silver disks ($d = 120$ nm, $h = 30$ nm). (a) Square lattice with 480 nm pitch; (b) rectangular lattice with 370 and 480 nm pitches; (c) hexagonal lattice with 555 nm nearest neighbor separation; and (d) honeycomb lattice with 320 nm nearest neighbor separation. Each of the structures has a lattice period of 480 nm.

The isolated particle extinction cross section was calculated using Eqs. (1), (2), (5), and (7), with optical constants for silver taken from the literature [30]. The extinction cross section of a particle in an array was calculated by additionally making use of Eqs. (1) and (4). Figure 1 shows that the single isolated particle has an optical response dominated by a resonance at ∼725 nm. When placed in the array the response changes dramatically, a sharp spectral feature appearing at ∼770 nm.

In this work we look at how the optical response (transmission/extinction as a function of wavelength) of arrays based on square, hexagonal, honeycomb, and rectangular lattices differ from each other. Scanning electron micrographs (SEMs) of the different particle arrangements fabricated are shown in Fig. 2. The lattices were designed so that the spectral position of the diffraction edge of each of the structures was the same. Each of the structures had a period of 480 nm so that the diffraction edge was at 727 nm (the array is index matched in oil with $n = 1.515$).

II. FABRICATION

Array fabrication was based on EBL, with silver nanoparticle arrays (50 μm × 50 μm) being made on glass substrates [there was no conductive (ITO) layer under the particles]. The substrates were first cleaned with acetone and propan-2-ol. They were then dried in a nitrogen stream, spin coated with 950k A4 poly(methyl methacrylate) (PMMA) resist at 4000 rpm, and baked for 20 min at 160 °C. EBL was then used to expose the resist to various array patterns, and the resist was then processed by chemical development to leave holes in the resist where exposure to the electron beam had taken place. Silver was then deposited by thermal evaporation

at 2×10^{-6} mbar and a rate of 2 Å s^{-1}. The mass of silver deposited was monitored with a quartz crystal microbalance from which the deposited thickness was calculated—a film thickness of 30 nm was used. Finally, lift off was achieved by placing the sample in warm acetone for 2–10 min, followed by a rinse in propan-2-ol, and dried in a nitrogen stream. This procedure produced particles of 120 nm $\pm 10\%$ in diameter and 30 nm $\pm 10\%$ in height.

III. CHARACTERIZATION

The optical extinction was calculated from $1 - T$, where T is the measured transmittance and is given by

$$T = \frac{\text{signal} - \text{background}}{\text{reference} - \text{background}}, \tag{8}$$

where the *signal* is the measured transmission of the array and substrate, the *background* is the dark counts of the CCD, and the *reference* is the transmission of a blank portion of the substrate. Extinction measurements were made with a Nikon ECLIPSE TE2000-U inverted microscope coupled to an Acton Research Corporation Spectra Pro-2500i spectrometer with a spectral resolution of 1 nm. A halogen lamp source ($\lambda =$ 400–1000 nm) with a linear polarizer was used. The beam spot on the sample was reduced to a diameter of 30 μm by inserting a pinhole aperture between the light source and the condenser, thereby giving a beam divergence of less than 1 deg. The arrays were then index matched with oil ($n = 1.515$) [31,32] and the transmitted light collected with an oil immersion lens (NA of 1.25). A long-pass filter (cutoff 500 nm) was inserted in the optical path after the collection objective to remove higher diffracted orders.

IV. RESULTS AND DISCUSSION

Let us first look at the data from the square array. Figure 3 shows (a) the measured extinction, (b) the calculated extinction cross section per particle, and (c) the calculated real and imaginary parts of the array factor S of a 480 nm pitch square array of silver disks ($d = 120$ nm, $h = 30$ nm). The inverse polarizability of a single disk is shown on the same plot as the array factor. The electric field is linearly polarized and is parallel to the y axis, see Fig. 2(a). It should be noted that the array factor has been smoothed using a cubic spline approach [33]. Dashed lines in Figs. 3(a) and 3(b) indicate the intersection of the real parts of $1/\alpha$ and S. In the measured extinction for a square lattice of silver particles, see Fig. 3(a), two peaks dominate the extinction spectrum, one at ~650 nm, the other at ~755 nm, we attribute these peaks to SLRs. The dip at ~520 nm is due to the $\langle 1,1 \rangle$ diffracted order and the small peak at ~720 nm is usually attributed to divergence of the illumination beam [16]. From the calculations, see Fig. 3(b), two SLRs are apparent, occurring at ~660 and ~770 nm, with the single isolated particle resonance at ~725 nm. These SLRs correspond to the spectral positions for which the real part of $1/\alpha$ intersects the real part of S [7], see Eq. (3). Provided the difference between the imaginary parts of $1/\alpha$ and S are small, the intersection of the real parts corresponds closely to the calculated extinction maximum, this is the case for the SLR at ~770 nm. When the difference between the

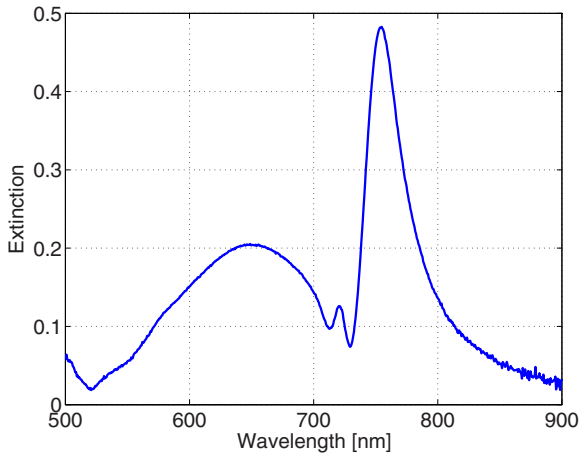

(a) Measured extinction spectrum

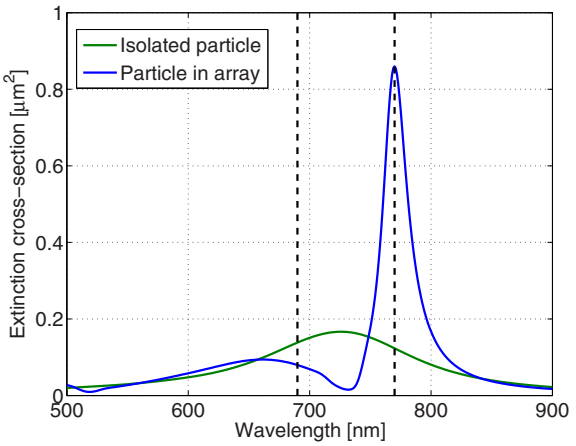

(b) Calculated extinction cross-section per particle

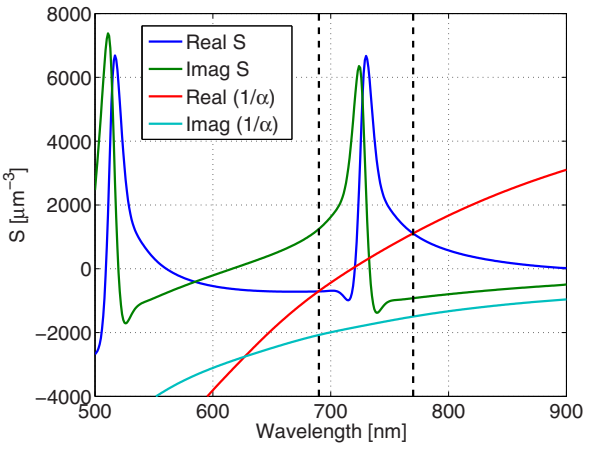

(c) $1/\alpha$ and S

FIG. 3. (Color online) (a) Measured extinction; (b) calculated extinction cross section per particle; and (c) array factor for a square array (480 nm pitch) of silver disks ($d = 120$ nm, $h = 30$ nm). The particles are illuminated with linearly polarized light at normal incidence with the electric field parallel to the y axis of the array, see Fig. 2(a). The array is index matched using immersion oil with $n = 1.515$, meaning that the diffraction edge is at 727 nm. Dashed lines in (a) and (b) indicate the intersection of the real parts of $1/\alpha$ and S.

imaginary parts of $1/\alpha$ and S are not small, the calculated extinction peak will, in general, be somewhat shifted from the position at which the real parts intersect, this is the case for the SLR at 690 nm. There is a third crossing point at ∼720 nm but no resonance is seen at this spectral position due to the significant difference between the imaginary parts of $1/\alpha$ and S [8,34]. We also observe that the SLR at ∼755 nm is much stronger and narrower than the SLR at ∼660 nm due to the smaller difference between the imaginary parts of $1/\alpha$ and of S.

Let us now turn to the hexagonal array. Figure 4 shows (a) the measured extinction, (b) the calculated extinction per particle, and (c) the array factor for a hexagonal lattice, see Fig. 2(c), of silver disks ($d = 120$ nm, $h = 30$ nm), together with the inverse polarizability of an isolated particle with the same dimensions. The hexagonal lattice has a nearest neighbor separation of 555 nm and is illuminated with an electric field parallel to the y axis of the array, see Fig. 2(c). As for the square array, two SLRs at ∼635 and ∼760 nm can be seen in the measured extinction spectrum of the hexagonal array, Fig. 4(a). Two SLRs can also be seen in the calculated spectra, Fig. 4(b), but these occur at somewhat different wavelengths (∼645 and ∼778 nm, respectively). Again, the SLRs occur when the real part of $1/\alpha$ intersects the real part of S, this can be seen in Fig. 4(c) (679 nm, 779 nm). The calculations in Figs. 4(b) and 4(c) are performed following the same procedure adopted for the square lattice. Similar results for hexagonal arrays have been predicted by Zou *et al.* [8] and experimentally obtained by Haynes *et al.* [34].

Figure 5 shows the extinction and array factors for a honeycomb lattice with a 320 nm nearest neighbor separation shown in Fig. 2(d). The particles are silver disks ($d = 120$ nm, $h = 30$ nm) and are index matched with $n = 1.515$ immersion oil. Figure 5(a) is the measured extinction, Fig. 5(b) is the calculated extinction, and Fig. 5(c) is the array factor with the calculated inverse polarizability for a single isolated particle. From Fig. 5(a) we see that there are two main peaks present in the spectrum. These peaks occur at ∼650 and ∼743 nm and are the SLRs associated with the array. These SLRs can also be seen in the calculated spectrum, Fig. 5(b), but occurring at somewhat different wavelengths (∼665 and ∼753 nm, respectively). Again, these SLRs occur when the real part of S intersects the real part of $1/\alpha$, see Fig. 5(c) (684 nm, 753 nm).

In Fig. 6 we compare the measured extinction and the real parts of the array factors for square, hexagonal, and honeycomb arrays. Each of the arrays consist of silver disks (120 nm diameter and 30 nm height) surrounded by a refractive index $n = 1.515$. Figure 6(a) shows the measured extinction while Fig. 6(b) shows the real part of the corresponding array factors with the real part of $1/\alpha$ of a silver disk ($d = 120$ nm, $h = 30$ nm) also included. We see from Fig. 6(a) that even though all three lattice types have their diffraction edge in the same position, the strongest SLR of the arrays occurs at slightly different spectral positions for each: ∼743 nm for honeycomb, ∼755 nm for square, and ∼760 nm for hexagonal. These differences can be understood by looking at the real parts of S and $1/\alpha$ shown in Fig. 6(b). Here one sees that the real part of $1/\alpha$ intersects the real part of S for the different lattice types at slightly different positions: ∼753 nm for honeycomb, ∼770 nm for square, and ∼779 nm for hexagonal. The real part of S for each of these arrays is different because S [Eq. (4)] is

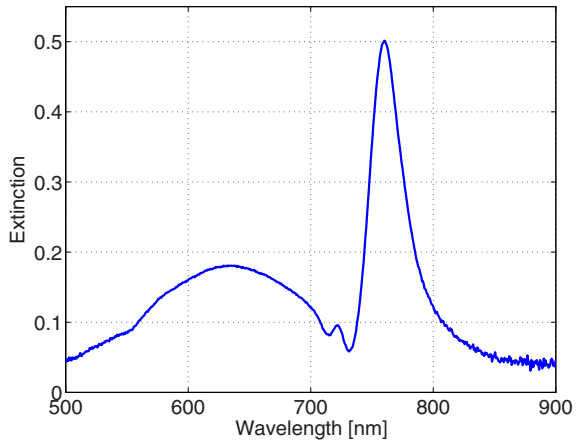

(a) Measured extinction spectrum

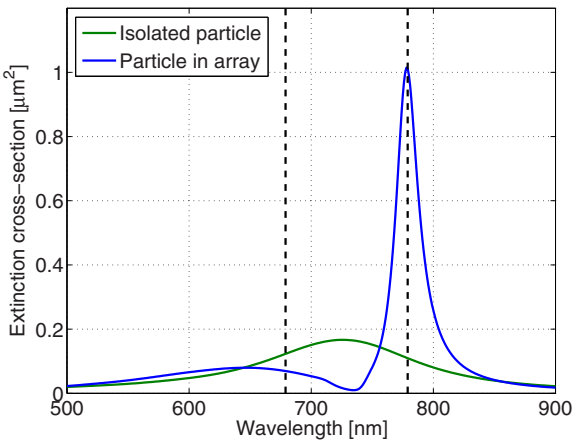

(b) Calculated extinction cross-section per particle

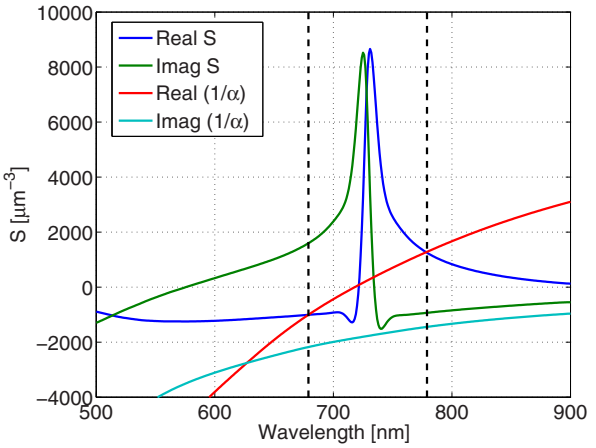

(c) $1/\alpha$ and S

FIG. 4. (Color online) (a) Measured extinction; (b) calculated extinction cross section per particle; and (c) array factor for a hexagonal array (555 nm nearest neighbor separation) of silver disks ($d = 120$ nm, $h = 30$ nm). The particles were illuminated with linearly polarized light at normal incidence with an electric field parallel to the y axis of the array, see Fig. 2(c).

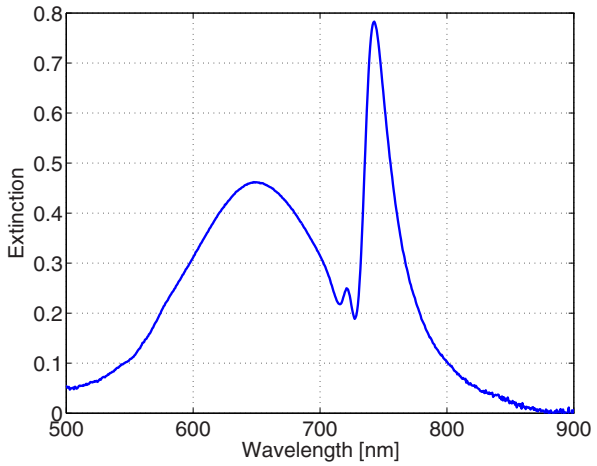

(a) Measured extinction spectrum

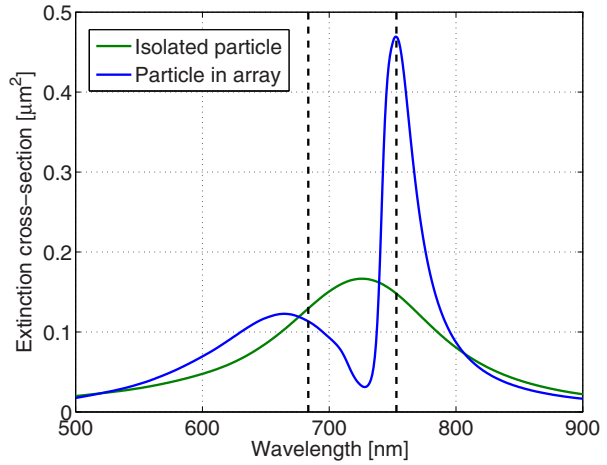

(b) Calculated extinction cross-section per particle

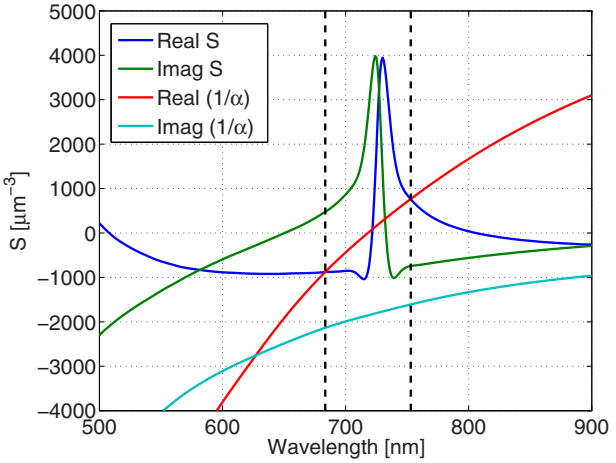

(c) $1/\alpha$ and S

FIG. 5. (Color online) (a) Measured extinction; (b) calculated extinction cross section per particle; and (c) array factor for a honeycomb lattice (320 nm nearest neighbor separation) of silver disks ($d = 120$ nm, $h = 30$ nm). The particles are illuminated with linearly polarized light at normal incidence with the electric field parallel to the y axis of the array, see Fig. 2(d).

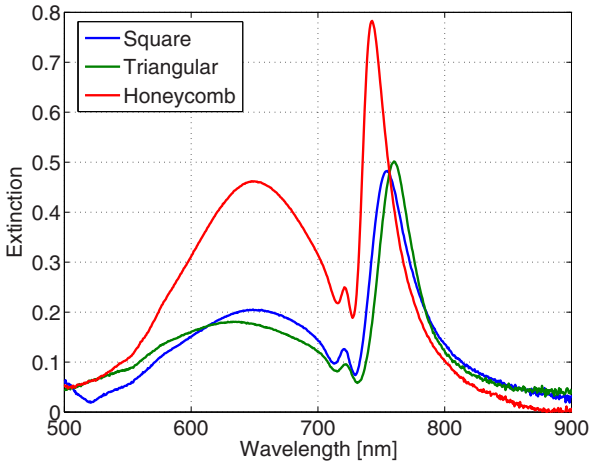

(a) Measured extinction

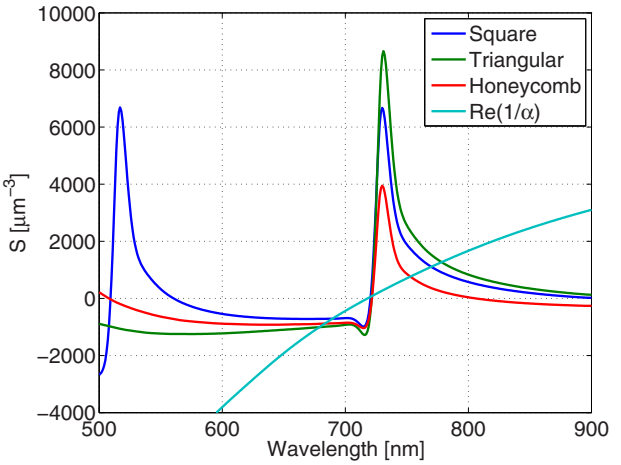

(b) Real parts of $1/\alpha$ and S

FIG. 6. (Color online) (a) Measured extinction of square lattice [see Fig. 2(a)], hexagonal lattice [see Fig. 2(c)], and honeycomb lattice [see Fig. 2(d)] with corresponding real parts of $1/\alpha$ and S shown in (b).

different for each of the lattice types; it depends on the position of the particles in the lattice. In Fig. 6(a) the honeycomb lattice has the greatest extinction, due to this array having a greater number of particles per unit area than the two other array types. In Fig. 6(b) the square lattice has an additional feature due to the $\langle 1,1 \rangle$ diffraction edge.

The square, hexagonal, and honeycomb lattices all have a high degree of symmetry. As a consequence we expect their optical response (extinction) to be independent of the orientation (polarization) of the incident electric field. To check this, extinction spectra are plotted as a function of wavelength, see Fig. 7, for the three particle array types. In each case, the orientation of the electric field is swept in 15 deg increments from 0 deg (parallel to the x axis of the arrays) to 90 deg (parallel to the y axis). The response of all three lattices are found to be insensitive to the orientation of the incident electric field, as expected from their high degree of symmetry.

To investigate further how the particles in an array couple together it is instructive to look at a lower symmetry lattice;

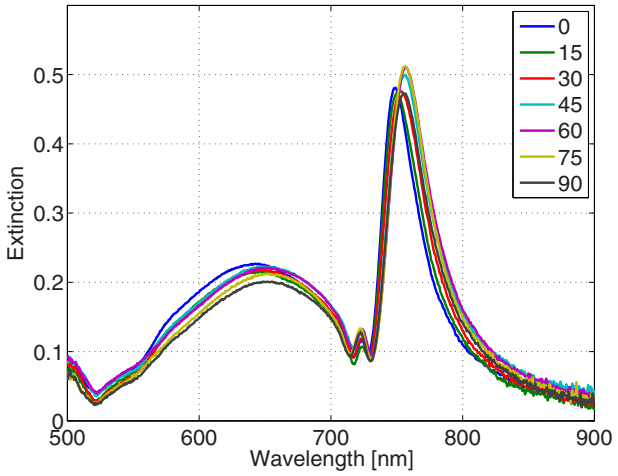

(a) Square

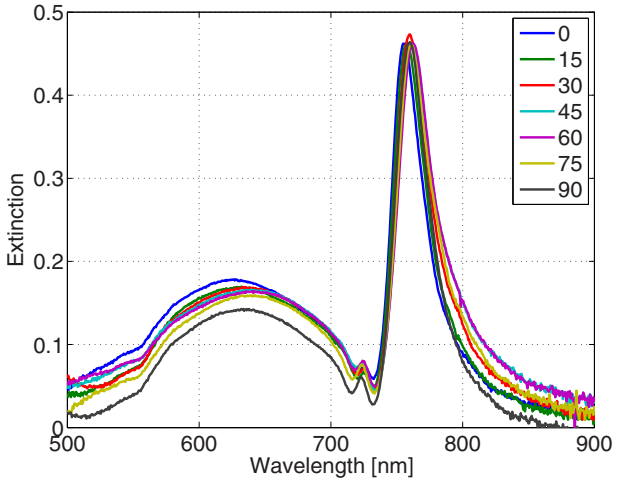

(b) Hexagonal

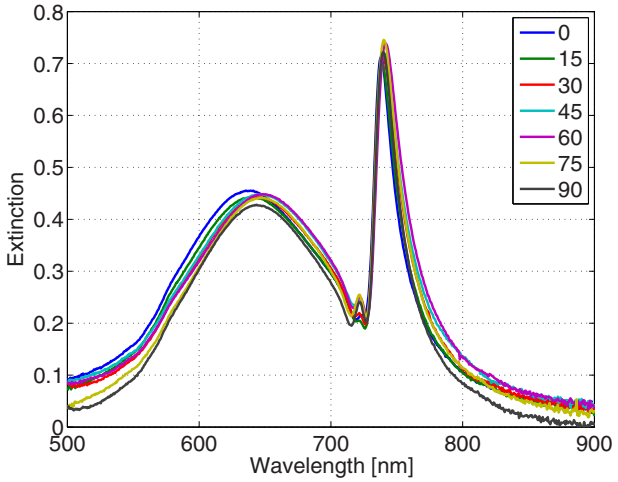

(c) Honeycomb

FIG. 7. (Color online) Measured extinction vs wavelength (nm) of the three different geometries: (a) square, (b) hexagonal, and (c) honeycomb. In each case, the electric field polarization is swept in 15 deg increments from 0 deg (parallel to the x axis of the arrays) to 90 deg (parallel to the y axis).

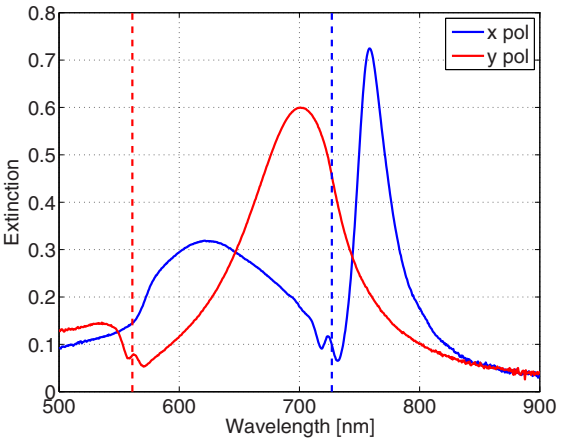

(a) Measured extinction spectrum

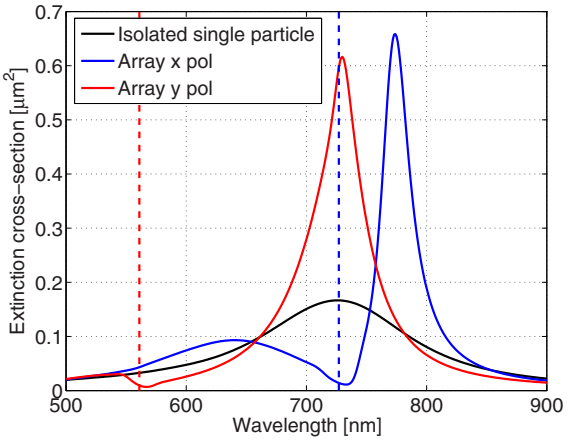

(b) Calculated extinction cross-section per particle

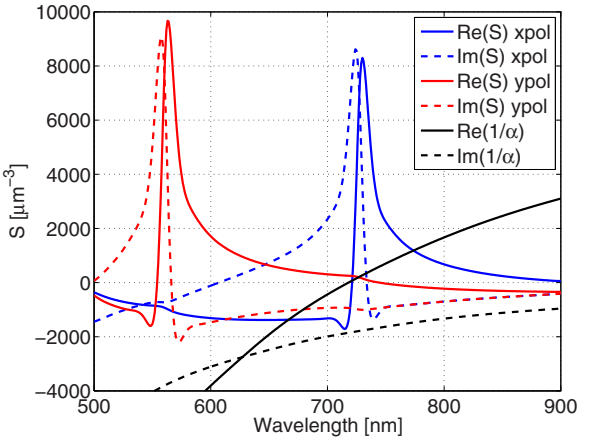

(c) $1/\alpha$ and S

FIG. 8. (Color online) (a) Measured extinction; (b) calculated extinction cross section per particle; and (c) array factor for a rectangular lattice (370 nm × 480 nm pitches) of silver disks ($d = 120$ nm, $h = 30$ nm), together with the calculated inverse polarizability of an isolated particle. The particles were illuminated with linearly polarized light at normal incidence with the electric field parallel to either the x axis or y axis of the array, see Fig. 2(b). The array is index matched using immersion oil with $n = 1.515$. The two diffraction edges occur at 561 nm (red dashed line) and 727 nm (blue dashed line).

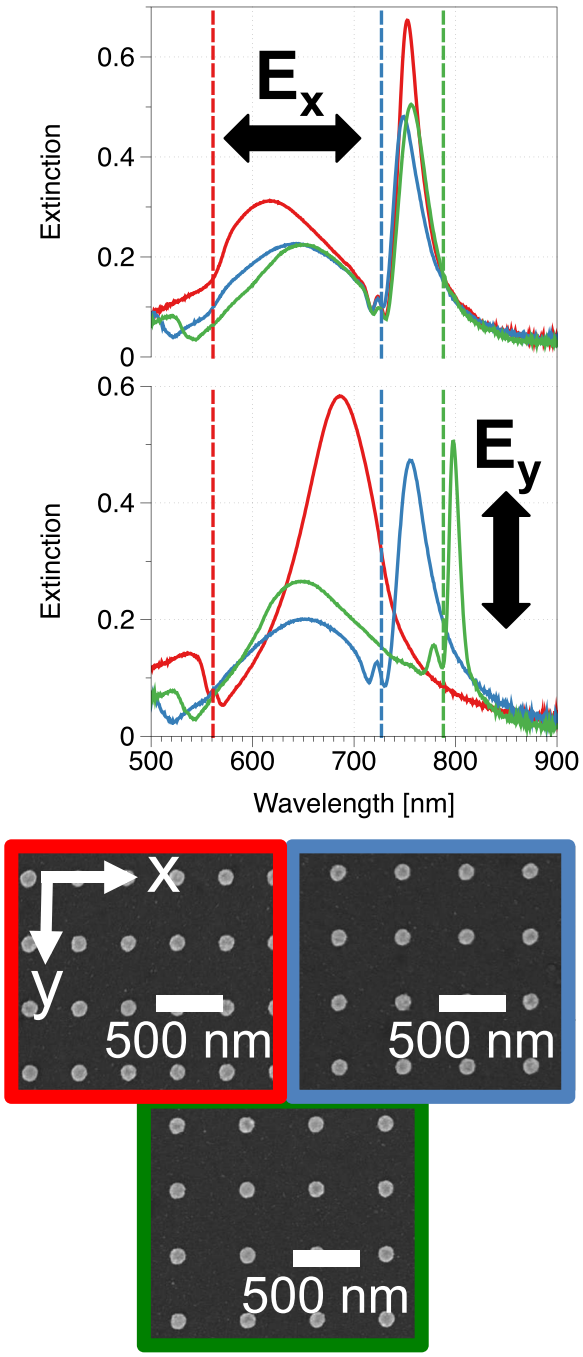

FIG. 9. (Color online) Measured extinction as a function of wavelength of a 370 nm × 480 nm rectangular lattice, 480 nm pitch square lattice, and 520 nm × 480 nm rectangular lattice. All the lattices consist of silver disks with a diameter of 120 nm and height of 30 nm. The top panel is with electric field parallel to the x axis of the array and middle panel the y axis. The diffraction edges relating to the y period of the three lattices are shown as dashed lines at 561 nm (red), 727 nm (blue), and 788 nm (green).

the rectangular lattice. Figure 8 shows data for a rectangular array (370 nm × 480 nm pitches) of silver disks ($d = 120$ nm, $h = 30$ nm) with $n = 1.515$, see Fig. 2(b). Figure 8(a) shows the measured extinction for the electric field parallel to the x axis and for the electric field parallel to the y axis; Fig. 8(b) for the calculated extinction; and Fig. 8(c) for the calculated array factor, together with the calculated inverse polarizability of an isolated particle. When the electric field is parallel to the x axis we see two SLRs in the measured extinction at ∼620 and ∼758 nm, Fig. 8(a). A very different response is obtained when the electric field is parallel to the y axis, giving just one SLR at ∼701 nm. In the calculated extinction, Fig. 8(b), the positions of the SLRs occur at ∼640 and ∼774 nm when the electric field is parallel to the x axis and at ∼730 nm for the electric field parallel to the y axis. The calculated position of these SLRs correspond to the crossing of the real part of $1/\alpha$ with the real part of S, as seen in Fig. 8(c). As for the square, hexagonal, and honeycomb arrays, the calculated position of the extinction maximum best matches the crossing point of the real part of $1/\alpha$ and S when the difference in the imaginary parts is small. The key observation we can make from the data shown in Fig. 8(a) is that the response is dramatically different for the two illumination polarizations. To explore this further we investigated the response from a number of different rectangular arrays.

Figure 9 shows the measured extinction vs wavelength of two rectangular arrays and a square array. In all three arrays the y period has been kept constant at 480 nm while the x period has been changed. The x period of the arrays are 370 nm (red), 480 nm (blue), and 520 nm (green). The top panel of the figure is for the electric field parallel to the x axis and the middle panel for the electric field parallel to the y axis. When the electric field is parallel to the x axis, a very similar response is obtained for the three arrays with their SLRs at ∼748, ∼753, and ∼756 nm. If the polarization is now changed to be along the y axis (bottom panel), three very different spectra are seen (middle panel). As the diffraction edge is moved to longer wavelengths, this pushes the SLR to longer wavelengths. For the 370 nm y pitch the SLR occurs at ∼685 nm; for the 480 nm y pitch the SLR occurs at ∼755 nm; and for the ∼520 nm y pitch the SLR occurs at ∼798 nm. The difference in response for the two different polarizations of the incident field can be understood by considering the nature of the coupling between neighboring particles. This coupling, for the particle separations considered here, is far field in character [35]. The dipolar far field is strongest in the direction perpendicular to the dipole moment, the important distance is thus the particle separation in the direction perpendicular to the incident electric field.

V. CONCLUSION

In summary, arrays of silver nanoparticles have been fabricated by electron-beam lithography. We have shown that the optical response (transmission) of an array of particles, whose array period is similar to the particle plasmon resonance wavelength, differs dramatically from that of an isolated single particle of the same material and dimensions. We have shown that square, rectangular, hexagonal, and honeycomb arrays all show strong surface lattice resonances, and that the main SLRs occur at slightly different spectral positions with different strengths, even though all of the lattices have the same diffraction edge. These differences can be explained by looking at the different array factors that apply in each case, i.e., by looking at how the net field at the site of any given particle depends on the arrangement of particles around

it. For the arrays considered here, we find that the period of the structure is more important than the nearest neighbor separation in determining the response of the array. The exact position of the SLR is determined by the point of intersection of the real part of the inverse single particle polarizability $1/\alpha$ and the real part of the array factor S. The strength and the width of the SLR depends on the difference between the imaginary part of α and the imaginary part of S and the angle of intercept between the real part of α and the real part of S. From the results presented here there is not much to choose between the array types when looking to see which array type gives the narrower SLR. Finally, by studying rectangular arrays we demonstrated that particles in wavelength-scale arrays couple together in the direction perpendicular to the applied electric field.

We hope that our findings may be useful to those seeking to exploit wavelength-scale plasmonic particle arrays in a number of areas, for example, sensing [36] and lasers [37]. Finally, we note that the SLRs might also arise as a result of exciton rather than plasmonic resonances [24].

ACKNOWLEDGMENTS

A.D.H. would like to thank Dr. N. Meinzer for help with fabrication and for useful discussions, and N. Cole for technical help. This work was supported in part by the Royal Society through their International Exchange Scheme, and by The Leverhulme Trust.

[1] S. Zou and G. C. Schatz, Chem. Phys. Lett. **403**, 62 (2005).
[2] J. J. Mock, M. Barbic, D. R. Smith, D. A. Schultz, and S. Schultz, J. Chem. Phys. **116**, 6755 (2002).
[3] W. A. Murray and W. L. Barnes, Adv. Mater. **19**, 3771 (2007).
[4] W. A. Murray, J. R. Suckling, and W. L. Barnes, Nano Lett. **6**, 1772 (2006).
[5] K. T. Carron, W. Fluhr, M. Meier, A. Wokaun, and H. W. Lehmann, J. Opt. Soc. Am. B **3**, 430 (1986).
[6] V. A. Markel, J. Mod. Opt. **40**, 2281 (1993).
[7] V. A. Markel, J. Phys. B: At. Mol. Opt. Phys. **38**, L115 (2005).
[8] S. Zou and G. C. Schatz, J. Chem. Phys. **121**, 12606 (2004).
[9] B. Lamprecht, G. Schider, R. T. Lechner, H. Ditlbacher, J. R. Krenn, A. Leitner, and F. R. Aussenegg, Phys. Rev. Lett. **84**, 4721 (2000).
[10] E. M. Hicks, S. Zou, G. C. Schatz, K. G. Spears, R. P. Van Duyne, L. Gunnarsson, T. Rindzevicius, B. Kasemo, and M. Käll, Nano Lett. **5**, 1065 (2005).
[11] J. Sung, E. M. Hicks, R. P. Van Duyne, and K. G. Spears, J. Phys. Chem. C **112**, 4091 (2008).
[12] V. G. Kravets, F. Schedin, and A. N. Grigorenko, Phys. Rev. Lett. **101**, 087403 (2008).
[13] B. Auguié and W. L. Barnes, Phys. Rev. Lett. **101**, 143902 (2008).
[14] Y. Chu, E. Schonbrun, T. Yang, and K. B. Crozier, Appl. Phys. Lett. **93**, 181108 (2008).
[15] B. Auguié and W. L. Barnes, Opt. Lett. **34**, 401 (2009).
[16] S. Rodriguez, M. Schaafsma, A. Berrier, and J. Gómez Rivas, Physica B **407**, 4081 (2012).
[17] W. Zhou and T. W. Odom, Nat. Nanotechnol. **6**, 423 (2011).
[18] V. Giannini, G. Vecchi, and J. Gómez Rivas, Phys. Rev. Lett. **105**, 266801 (2010).
[19] S. R. K. Rodriguez and J. Gómez Rivas, Opt. Express **21**, 27411 (2013).
[20] A. I. Väkeväinen, R. J. Moerland, H. T. Rekola, A.-P. Eskelinen, J.-P. Martikainen, D.-H. Kim, and P. Törmä, Nano Lett. **14**, 1721 (2014).
[21] P. Lunnemann, I. Sersic, and A. F. Koenderink, Phys. Rev. B **88**, 245109 (2013).
[22] L. Malassis, P. Massé, M. Tréguer-Delapierre, S. Mornet, P. Weisbecker, P. Barois, C. R. Simovski, V. G. Kravets, and A. N. Grigorenko, Adv. Mater. **26**, 324 (2014).
[23] C. F. Bohren and D. R. Huffman, *Absorption and Scattering of Light by Small Particles* (Wiley-VCH, Berlin, 2004).
[24] M. G. Gentile, S. Núñez Sánchez, and W. L. Barnes, Nano Lett. **14**, 2339 (2014).
[25] U. Kreibig and M. Vollmer, *Optical Properties of Metallic Clusters* (Springer, New York, 1995).
[26] M. Meier and A. Wokaun, Opt. Lett. **8**, 581 (1983).
[27] A. Wokaun, J. P. Gordon, and P. F. Liao, Phys. Rev. Lett. **48**, 957 (1982).
[28] A. Moroz, J. Opt. Soc. Am. B **26**, 517 (2009).
[29] F. J. García de Abajo, Rev. Mod. Phys. **79**, 1267 (2007).
[30] D. W. Lynch and W. R. Hunter, in *Handbook of Optical Constants of Solids*, edited by E. D. Palik (Academic, New York, 1985), pp. 275–367.
[31] B. Auguié, X. M. Bendaña, W. L. Barnes, and F. J. García de Abajo, Phys. Rev. B **82**, 155447 (2010).
[32] A. G. Nikitin, T. Nguyen, and H. Dallaporta, Appl. Phys. Lett. **102**, 221116 (2013).
[33] Smoothing was carried out using MATLAB function "csaps" with a smoothing parameter of 0.01.
[34] C. L. Haynes, A. D. Mcfarland, L. Zhao, R. P. V. Duyne, G. C. Schatz, L. Gunnarsson, J. Prikulis, B. Kasemo, and M. Kall, J. Phys. Chem. B **107**, 7337 (2003).
[35] A. Pinchuk and G. Schatz, Mater. Sci. Eng. B **149**, 251 (2008).
[36] V. G. Kravets, F. Schedin, R. Jalil, L. Britnell, R. V. Gorbachev, D. Ansell, B. Thackray, K. S. Novoselov, A. K. Geim, A. V. Kabashin, and A. N. Grigorenko, Nat. Mater. **12**, 304 (2013).
[37] J. Stehr, J. Crewett, F. Schindler, R. Sperling, G. von Plessen, U. Lemmer, J. Lupton, T. Klar, J. Feldmann, A. Holleitner, M. Forster, and U. Scherf, Adv. Mater. **15**, 1726 (2003).